IOP Publishing Plasma Physics and Controlled Fusion

Plasma Phys. Control. Fusion **58** (2016) 034010 (7pp) doi:10.1088/0741-3335/58/3/034010

Pico-coulomb charge measured at BELLA to percent-level precision using a Turbo-ICT

K Nakamura[1], D E Mittelberger[1], A J Gonsalves[1], J Daniels[1], H-S Mao[1], F Stulle[2], J Bergoz[2] and W P Leemans[1]

[1] Lawrence Berkeley National Laboratory, Berkeley, CA 94720, USA
[2] Bergoz Instrumentation, 01630 Saint-Genis-Pouilly, France

E-mail: KNakamura@lbl.gov and stulle@bergoz.com

Received 31 July 2015, revised 12 November 2015
Accepted for publication 16 December 2015
Published 9 February 2016

Abstract

Precise diagnostics of picocoulomb level particle bunches produced by laser plasma accelerators (LPAs) can be a significant challenge. Without proper care, the small signals associated with such bunches can be dominated by a background generated by laser, target, laser–plasma interaction and particle induced radiation. In this paper, we report on first charge measurements using the newly developed Turbo-ICT for LPAs. We outline the Turbo-ICT working principle, which allows precise sub-picocoulomb measurements even in the presence of significant background signals. A comparison of the Turbo-ICT, a conventional integrating current transformer (ICT) and a scintillating screen (Lanex) was carried out at the Berkeley Lab Laser Accelerator. Results show that the Turbo-ICT can measure sub-picocoulomb charge accurately and has significantly improved noise immunity compared to the ICT.

Keywords: laser plasma accelerator, charge diagnostics, Lanex, Turbo-ICT, ICT

(Some figures may appear in colour only in the online journal)

1. Introduction

Laser plasma accelerators (LPAs) have shown great potential for the realization of compact high energy particle accelerators [1, 2]. Their unique operating mode and properties of the produced particle bunches impose new challenges on particle beam diagnostics. At the present time, depending on the operating conditions, LPA particle beams can have a significant energy spread (few % to 100% level), angular divergence (mrad to sub-mrad level) and charge jitter (a few 10's of %). They can also be accompanied by low-energy non-relativistic electron clouds. Additionally, the devices that create the gas/plasma target (e.g. pulsed gas jets or high voltage capillary discharge systems) and the laser–plasma interaction itself can induce electromagnetic pulses (EMP) that are either picked up directly by beam diagnostics or, indirectly, via cables or other parts of the installation. Particles lost along the beamline can scatter and produce secondary particles or x-rays. These effects can degrade the signals used to monitor the particle beam.

In order to reduce the charge measurement error, devices not susceptible to EMP, such as imaging plates and scintillating screens, have been widely used in LPAs [3–5]. In addition to the beam charge, they can measure the beam profile and pointing as well. However, these devices affect the emittance of the beam passing through them and are susceptible to x-rays, which can erroneously contribute to charge determination.

Integrating current transformers (ICTs) [6] are commonly used in RF cavity-based accelerators for non-destructive charge measurements. In LPA environments, ICTs can overestimate the charge by more than an order of magnitude [4, 5] if not used under the proper conditions. However, a previous study using a gas-jet based LPA showed that, with special care to reduce the detrimental influence of the EMP and other noise sources described above, an ICT can provide accurate charge information for 5 pC and above [7]. The limitation on minimum charge was due to noise on the ICT signal.

The severity of the noise can depend on the choice of plasma target. A capillary-discharge waveguide [8], which can increase the beam energy of LPAs [9–11], produces additional EMP noise that increases the difficulty in using ICTs. A device to perform non-destructive charge measurements of

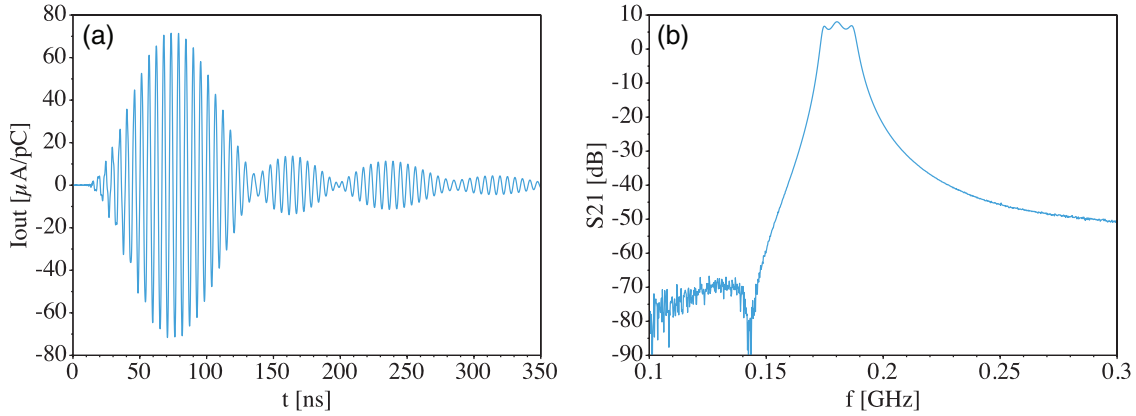

Figure 1. (a) Expected output signal of the Turbo-ICT installed at BELLA in time-domain. (b) The transmission coefficient $S_{21}(f)$ measured by a vector network analyzer for the Turbo-ICT installed at BELLA.

LPA electron beams with higher resolution (sub-picocoulomb) and better noise immunity has been highly desired, especially for future applications of LPAs such as free electron lasers that operate with picocoulomb bunches.

A new device, the Turbo-ICT, has recently been developed to accurately measure the charge of electron beams used in x-ray free-electron lasers (X-FELs) and from LPAs. The Turbo-ICT is accompanied by an RF electronics card for beam charge monitoring (BCM-RF). Together they operate in a manner that makes them intrinsically less susceptible to external noise sources. Promising experimental results were reported measuring the charge from an RF cavity based accelerator at the Pohang Accelerator Laboratory Injector Test Facility [12]. The ICT, the Turbo-ICT and the Lanex screen have different potential sources of noise that can affect the charge measurement. Therefore a comparison of these diagnostics is useful for evaluation and mitigation of these noise sources. In this paper, the use of the Turbo-ICT, in environments that have high levels of electrical noise, is demonstrated through a charge diagnostics comparison using the Berkeley Lab Laser Accelerator (BELLA) petawatt beamline at the Lawrence Berkeley National Laboratory [11].

2. Working principle of ICT and Turbo-ICT

In RF particle accelerators, the charge of the particle bunches is usually measured non-destructively using current transformers. These transformers inductively measure the beam current. Integration yields a value proportional to charge. Proportionality factors depend on transformer characteristics and can be accurately determined in the laboratory. Importantly, to obtain integrable pulses the ICT must cover a spectrum containing near-DC frequency, roughly ranging from kHz to MHz. For example, a conventional ICT installed at BELLA petawatt beam line (10.0 Vs C^{-1} sensitivity model) had a spectrum cut-off at 11 MHz.

The Turbo-ICT is a combination of a high-frequency current transformer and a narrow band-pass filter. As detailed in [14], the spectral response $Q_{out}(f)$ of a current transformer to an incoming current pulse $I_{in}(t)$ is the product of the incoming pulse's spectrum $Q_{in}(f)$ and the transmission coefficient $S_{21}(f)$ of the current transformer,

$$Q_{out}(f) = Q_{in}(f)S_{21}(f),$$

and the time-domain output current pulse $I_{out}(t)$ can be obtained from the inverse Fourier transform of $Q_{out}(f)$. The expected output signal of the Turbo-ICT installed at BELLA is shown in figure 1(a) in time-domain and (b) frequency-domain. One can see that the resonance frequency for this case was 180 MHz, and the bandwidth was approximately 15 MHz. These are typical values which can be adapted depending on accelerator requirements.

The apex of the output resonance is proportional to the input charge. It is measured by the BCM-RF electronics. The BCM-RF consists of a narrow band-pass filter and an amplifier. The band-pass filter eliminates the most of the noise that was picked by the cable between the Turbo-ICT and the BCM-RF. If the input pulse is considerably shorter than the resonance period, which is fulfilled in LPAs or X-FELs, the resonance apex is independent of other input pulse properties. A detailed description of the Turbo-ICT and BCM-RF working principle and their calibration is given in [14].

Usually, EMPs from LPAs are found to have quite broad bandwidth, from DC to above GHz, and to be highly variable. While the Turbo-ICT bandwidth is comparable to the ICT bandwidth, the center frequency was shifted to a higher frequency. More importantly, the BCM-RF provides band-pass filtering and signal amplification just before the signal digitization. This limits effect of the broadband EMP noise effectively and improves noise immunity.

3. Experimental setup for charge diagnostics comparison

In order to perform comparison of charge diagnostics, the Turbo-ICT was installed on the BELLA petawatt laser beam line together with a conventional ICT (10.0 Vs C^{-1} sensitivity) allowing simultaneous charge measurements of both ICTs and a scintillating screen. The experimental setup is illustrated in figure 2, and a schematic including laser diagnostics can

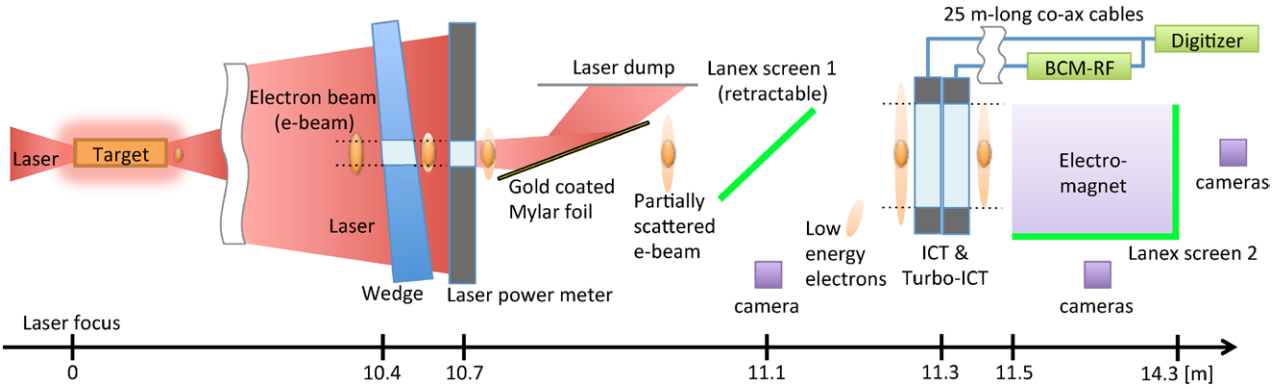

Figure 2. Schematic of the measurement setup. The limited clearance apertures created partially scattered electron beams. The Lanex screens, Turbo-ICT and ICT could capture different fractions of the beam depending on initial beam properties.

be found in [13]. Two types of target were used for comparison: a gas-jet target and a capillary-discharge target that are described in the following sections.

Electron beams generated at the laser-plasma interaction propagated in vacuum more than 10 meters without any magnetic transport and were aligned to pass through a fused silica wedge with a 25 mm diameter hole, followed by a laser power meter (consisting of glass and aluminum) also with a 25 mm diameter hole. The amount of beam passing through the holes depended on the systematic and shot-to-shot pointing errors, as well as beam divergence. The part of the laser pulse that passes through the holes was reflected by the gold-coated Mylar foil while allowing the electron beams to pass.

A scintillating screen (Lanex Fast front, Kodak, Rochester, NY, USA (noted as Lanex screen 1 in figure 2) was placed with a 45 degree angle with respect to the beam propagation axis, and the upstream side was covered with ~40 μm-thick aluminum foil to block the remnant laser light. The screen was placed on a retractable vacuum translation stage to study the effect of the screen on electron beams. The projected angle covered by the Lanex screen was 5.1 mrad horizontally by 7.2 mrad vertically. The light from the Lanex was imaged to a CCD camera (Flea3-GE-14S3M, Pointgrey, Canada), whose signal was calibrated to the beam charge in a previous study [7].

After passing through the Lanex screen 1, the electron beam went through the ICT and the Turbo-ICT. Both ICTs were fabricated into the same flange with 60 mm diameter aperture (ICT aperture), which provided the acceptance angle of 5.4 mrad. The ICT signal was directly measured with a digitizer (NI-USB 5133, National Instruments, USA). The signal from the Turbo-ICT was first sent to the BCM-RF, and its output was measured by the same digitizer as the ICT. Common-mode choke filters (CMCs) consisting of ferrites were installed in necessary locations to reduce noise, and shielded 25 m LMR200 cables were used for signal transfer. Both ICTs were calibrated prior to installation using their respective calibration procedures. All three diagnostics simultaneously measured the electron bunch charge.

The Turbo-ICT and ICT were located 0.2 m away from the electron spectrometer magnet. At that location, the strength of the stray field was measured to be 1.5% of the peak field. For sufficiently high operating fields inside the magnet, the

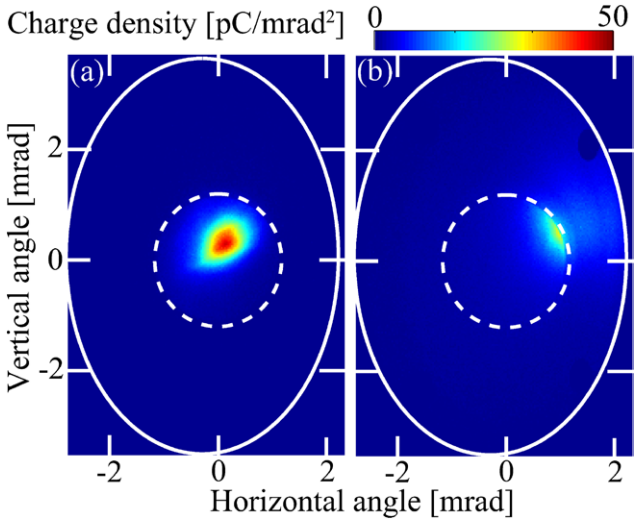

Figure 3. (a) Example Lanex image with more than 80% of the whole charge inside of the clearance angle. The charge measured within the clearance angle was 34 pC, and within whole Lanex screen was 40 pC. (b) Example Lanex image with less than 80% of the whole charge inside of the clearance angle. The charge measured within the clearance angle was 19 pC, and within whole Lanex screen was 56 pC. For both examples, the dashed white line indicates the clearance angle, and the solid white line indicates the Lanex screen.

magnet's fringe field can be strong enough to affect propagation of the low energy electrons. With the presence of the strong stray field, the low energy part of the beam that was measured by the Lanex screen could miss the ICTs as illustrated in figure 2. For example, based on trajectory calculations, the minimum electron momentum to go through the ICT aperture was 2.3 MeV/c for a 10 mT of stray field (corresponding peak magnetic field of 0.67 T). The stray field effect was studied experimentally with the electron beams from gas jet target and described in the following section.

The 25 mm diameter hole of the power meter defined clearance angle for the electron beam propagation, 2.4 mrad. For electron beams with divergence larger than the clearance angle and/or errors in electron beam pointing away from axis, the electron beam is scattered by the thick wedged optic and the laser power meter. Large angle scattered particles passing through the Lanex screen can hence miss the ICT aperture.

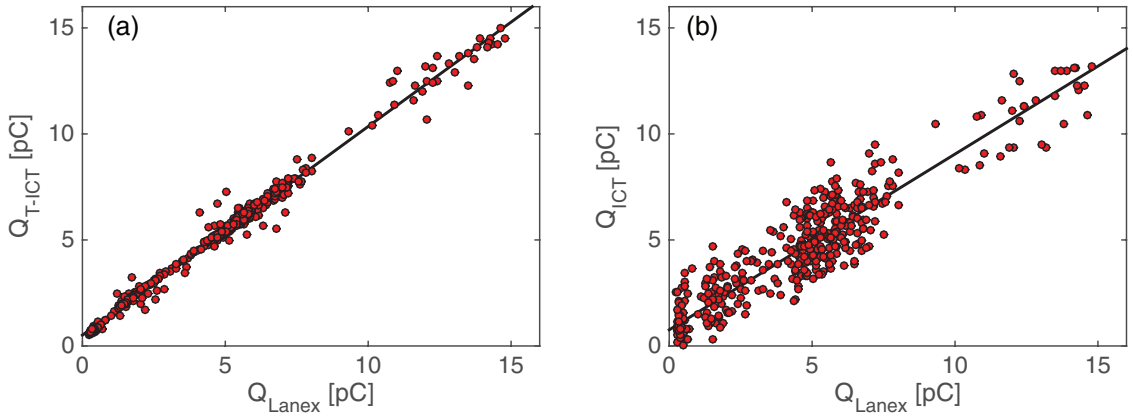

Figure 4. For a gas-jet based LPA, (a) charge measured by the Turbo-ICT versus by the Lanex screen and (b) charge measured by the ICT versus by the Lanex screen.

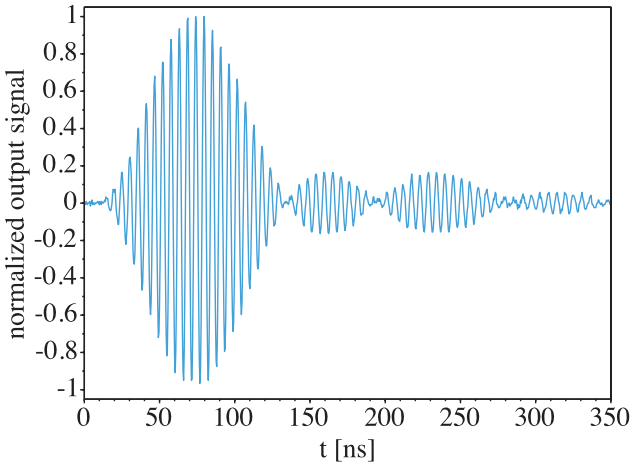

Figure 5. Normalized Turbo-ICT output signal measured on an oscilloscope.

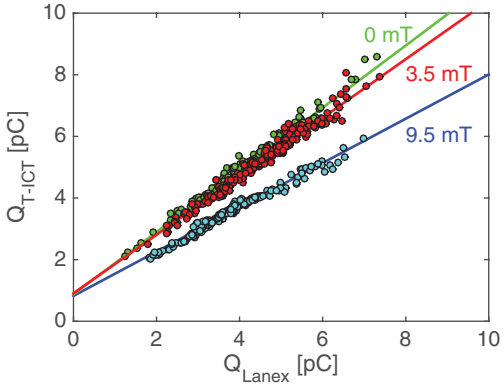

Figure 6. Charge measured by the Turbo-ICT versus by the Lanex screen for three different stray field. Shown by green circles are measurements for 0 mT stray field, and its linear fit is shown by the green solid line, The red circles and solid line for 3.5 mT case and the blue circles and solid line for 9.5 mT case, respectively.

A direct comparison of the amount of charge detected by the Lanex screen, Turbo-ICT and ICT is hence only accurate if the influence of the scattered part of the beam is negligible. In the data analysis, we therefore only considered electron beams that had more than 80% of the whole charge within the clearance aperture, as seen on the Lanex screen. Constraining the data to higher transmission ratios improves the correlation further but was not found to be necessary.

Shown in figure 3(a) is a Lanex image example that contained more than 80% of the charge within the clearance aperture. That particular bunch had 34 pC within the clearance aperture (indicated by the dashed white line), and about 40 pC when integrating over the entire Lanex screen (indicated by the solid white line). An example Lanex image for the beam that was rejected is shown in figure 3(b). The charge measured by the Lanex was obtained by integrating the charge within an elliptic region of 5.1 mrad horizontally (whole screen) by 5.4 mrad vertically, which was similar to the projection angle of the ICT aperture.

4. Results using a gas-jet target

A fast opening and closing gas jet valve from Alameda Applied Science Corporation [15] was used with a 15 mm long nozzle. Laser pulses of 13 J energy and peak power 330 TW were focused onto the middle of the hydrogen jet. To change the electron beam charge, the gas-jet density was varied to provide plasma electron density from $3 \times 10^{17}\,\mathrm{cm}^{-3}$ to $9 \times 10^{17}\,\mathrm{cm}^{-3}$. The observed electron beam energy spread ranged from below 50 MeV, which was the lower limit of the spectrometer measurements, to 1.5 GeV. The stray magnetic field at the ICTs was 3.5 mT.

Shown in figure 4(a) is the charge measured by the Turbo-ICT $Q_{\mathrm{T-ICT}}$ versus the charge measured by the Lanex screen Q_{Lanex}. The straight line in the plot is a linear fit,

$$Q_{\mathrm{T-ICT\,Fit}} = 0.98 Q_{\mathrm{Lanex}} + 0.51\,\mathrm{pC}.$$

The RMS data scatter about the fit was defined as $S_{\mathrm{T-ICT}} = \sqrt{\sum (Q_{\mathrm{T-ICT\,Fit}} - Q_{\mathrm{T-ICT}})^2 / n}$, and it was 0.21 pC. Both diagnostics are susceptible to noise, but since the sources of noise are different, significant noise will manifest as large data scatter $S_{\mathrm{T-ICT}}$. One can see that the correlation between the two diagnostics was excellent, even for charge below 5 pC. Since the observed $S_{\mathrm{T-ICT}}$ was low, the signal-to-noise ratios for both diagnostics were high, and bunch charge below 1 pC could be measured. The charge independent offset of approximately 0.5 pC between Lanex screen and Turbo-ICT

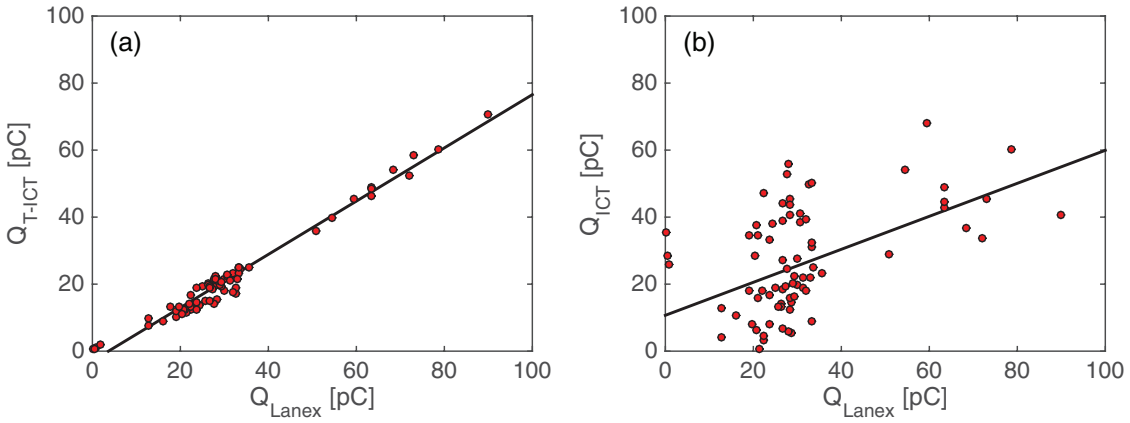

Figure 7. For a capillary-discharge based LPA, (a) charge measured by the Turbo-ICT versus by the Lanex screen and (b) charge measured by the ICT versus by the Lanex screen.

has been observed previously in [7] and is due to the detection threshold of the camera used to capture the Lanex screen images.

Figure 4(b) shows the charge measured by the ICT versus the charge measured by the Lanex screen. Note that the data sets shown in figure 4 were obtained using identical electron beams i.e. the measurements were done simultaneously. Again, a good correlation was observed, but with more scatter in the data than the Turbo-ICT measurements. The straight line in the plot is a linear fit,

$$Q_{\mathrm{ICT\,Fit}} = 0.83\ Q_{\mathrm{Lanex}} + 0.76\,\mathrm{pC}.$$

The higher RMS data scatter S_{ICT} 0.89 pC was observed and is primarily due to lower signal-to-noise ratio of the ICT measurements. A typical raw ICT signal was about a few mV with background noise of 0.34 mV (standard deviation). Note that a typical output from the BCM-RF was above 2 V with 10 mV background noise (standard deviation). Possible explanations for the reduced fit slopes are either charge dependent background signals impacting the ICT signal or a systematic error due to the fact that less than 10 points were sampled by the digitizer along the ICT output signal.

The improved measurement accuracy for the Turbo-ICT was clear from the comparison between figures 4(a) and (b), as well as the difference in the RMS data scatter. It was further examined by measuring its output signal directly on an oscilloscope, i.e. without using the BCM-RF and shown in figure 5. Within the measurement accuracy, the response agreed with the expected Turbo-ICT output signal (compare figure 1(a)). No influence of the EMP or other noise sources was visible thanks to the narrow-band response of the Turbo-ICT, well-shielded cables and CMCs.

As described in the previous section, the stray field from the magnetic spectrometer can deflect low energy electrons out of the ICT acceptance and can cause discrepancy between ICTs and Lanex screens. This effect was studied with the same gas jet target. The laser pulses of 12 J energy and peak power 310 TW were focused onto the middle of the hydrogen jet. The peak plasma electron density was fixed at $9 \times 10^{17}\,\mathrm{cm}^{-3}$ for this study, and the results are shown in figure 6. A linear fit was done in the same manner and the following were obtained,

$$Q_{\mathrm{T-ICT\,Fit}}(0\,\mathrm{mT}) = 1.0\ Q_{\mathrm{Lanex}} + 0.88\,\mathrm{pC},$$

$$Q_{\mathrm{T-ICT\,Fit}}(3.5\,\mathrm{mT}) = 0.95\ Q_{\mathrm{Lanex}} + 0.91\,\mathrm{pC},$$

$$Q_{\mathrm{T-ICT\,Fit}}(9.5\,\mathrm{mT}) = 0.72\ Q_{\mathrm{Lanex}} + 0.82\,\mathrm{pC}.$$

One can see that although the stray field effect was negligibly small for 3.5 mT case and it can be significant for higher stray field such as 9.5 mT where 28% reduction in the Turbo-ICT measurement was observed. Note that the experiments were done on different days and one can see consistency and reproducibility of the measurements from comparison of 3.5 mT cases shown in figures 4(a) and 6.

5. Results using a capillary-discharge target

To perform these experiments, a 9 cm long and 500 μm diameter capillary discharge target similar to the one described in [11, 13] was used. The gas flowing into the capillary was comprised of 1% nitrogen and 99% helium. Laser pulses of energy 13 J and peak power 330 TW were focused on the capillary entrance. The observed electron beam energy spread ranged from below 100 MeV, which was the lower limit of the spectrometer measurements, to 2.5 GeV.

During the measurements, the higher magnetic field was required to resolve higher energy electron beam, and the stray field at the ICT was 12 mT. The trajectory calculation indicated that the electrons with momenta up to 2.7 MeV/c were sufficiently deflected to miss the ICT aperture. Also the study on the stray field described in the previous section indicated that the non-negligible reduction in the measurements of the ICT and the Turbo-ICT is expected.

Figure 7(a) shows the charge measured by the Turbo-ICT versus the charge measured by the Lanex screen. One can see that the Turbo-ICT charge and Lanex charge were correlated very well, and the linear fit was

$$Q_{\mathrm{T-ICT\,Fit}} = 0.79 Q_{\mathrm{Lanex}} - 2.9\,\mathrm{pC}.$$

The absolute slope was found to be 20% lower than the gas jet experiments. This discrepancy was attributed to the stray magnetic field effect. Note that the amount of reduction

depends on the amount of charge contained in the low energy tail, which can vary between different experiments. Note also that the capillary target generated beams with the higher charge density than the gas jet target and that there possibly could be higher amounts of beam halo and fluctuations in charge in the regime in which the longer LPA target was operated. This will be investigated further in future experiments. Compared to the gas jet experiment, a somewhat higher value of the data scatter of 1.8 pC was observed. The major contribution to the data scatter can be attributed to a combination of Lanex screen camera noise, Turbo-ICT noise, and the scattered part of the beam.

For comparison, figure 7(b) shows the charge measured by the ICT versus the charge measured by the Lanex screen. The linear fits yielded:

$$Q_{\mathrm{ICT\,Fit}} = 0.49 Q_{\mathrm{Lanex}} + 10.7\,\mathrm{pC}.$$

The data set exhibited approximately 12 pC of data scatter. At low charge, this scatter can be attributed to the ICT. The r^2-coefficients of the fit in figure 7(b) was found to be low, 0.25 (i.e. the amount of data was insufficient for an accurate comparison). The high noise prevented the ICT from accurately measuring the charge from the capillary discharge based LPA.

6. Conclusions

A new charge diagnostic (Turbo-ICT) was tested using the BELLA petawatt beamline. Experiments were carried out to investigate the performance of the new Turbo-ICT and compare it to a Lanex screen and a conventional ICT. For these experiments a gas-jet target and a capillary-discharge target were used.

The experiments confirmed that all three diagnostics systems could reliably measure the charge produced by gas-jet based LPAs. For our experimental configuration, the scaling of charge between the three diagnostics was found to be $Q_{\mathrm{T-ICT\,Fit}} = 0.98 Q_{\mathrm{Lanex}} + 0.51\,\mathrm{pC}$ and $Q_{\mathrm{ICT\,Fit}} = 0.83 Q_{\mathrm{Lanex}} + 0.76\,\mathrm{pC}$. The low RMS data scatter for the Turbo-ICT (0.21 pC) was about four times better than the ICT results (0.89 pC), indicating clearly improved resolution, primarily due to the improved noise immunity from narrow-band property and improved signal treatment by the BCM-RF. This value sets an upper limit for the Turbo-ICT and Lanex screen noise. Hence, both were able to properly measure sub-picocoulomb charge, while the ICT was limited to measuring a few picocoulomb charge. The offset was attributed to the sensitivity of the camera, and the data scatter was attributed to the combination of Lanex screen noise, Turbo-ICT noise and partially scattered beam due to the limited clear aperture in the electron beam transport line.

In experiments using a capillary-discharge target, an excellent linear correlation of the Turbo-ICT and the Lanex screen was found, even when the ICT detected too much noise to measure the charge accurately. The scaling between Lanex and Turbo-ICT is given by $Q_{\mathrm{T-ICT\,Fit}} = 0.79 Q_{\mathrm{Lanex}} - 2.9\,\mathrm{pC}$. The deviation from unity in scaling can be attributed primarily to the systematic influence of the stray magnetic fields of the electron spectrometer on the electrons near the ICTs, which is an artifact of the particular experimental setup. However, the excellent correlation between the Turbo-ICT and the Lanex showed that Turbo-ICT experiments can be configured to accurately measure charges from capillary-discharge based LPAs.

Both sets of data showed that both the Lanex and the Turbo-ICT can measure charges down to the sub-picocoulomb level. While the Lanex has an advantage in a capability of measuring beam profile, the Turbo-ICT can measure charge in non-destructive manner. This ability is highly desirable for future applications of LPAs.

Acknowledgments

This work was performed as part of a collaboration between the BELLA Center, Lawrence Berkeley Laboratory and Bergoz Instrumentation. The work by the BELLA Center scientists and staff was supported by Office of Science, Office of HEP, US DOE under Contract DE-AC02-05CH11231 and the National Science Foundation. The authors gratefully acknowledge the contributions from Csaba Toth and technical support from Art Magana, Joe Riley, Aalhad Deshmukh, Dave Evans, Mark Kirkpatrick, Greg Mannino, Ken Sihler, Tyler Sipla, Don Syversrud and Nathan Ybarrolaza.

References

[1] Esarey E, Schroeder C B and Leemans W 2009 Physics of laser-driven plasma-based electron accelerators *Rev. Mod. Phys.* **81** 1229–85
[2] Macchi A, Borghesi M and Passoni M 2013 Ion acceleration by superintense laser-plasma interaction *Rev. Mod. Phys.* **85** 751–93
[3] Tanaka K A, Yabuuchi T, Sato T, Kodama R, Kitagawa Y, Takahashi T, Ikeda T, Honda Y and Okuda S 2005 Calibration of imaging plate for high energy electron spectrometer *Rev. Sci. Instrum.* **76** 013507
[4] Glinec Y, Faure J, Guemnie-Tafo A, Malka V, Monard H, Larbre J P, De Waele V, Marignier J L and Mostafavi M 2006 Absolute calibration for a broad range single shot electron spectrometer *Rev. Sci. Instrm.* **77** 103301
[5] Hidding B *et al* 2007 Novel method for characterizing relativistic electron beams in a harsh laser-plasma environment *Rev. Sci. Instrum.* **78** 083301
[6] Unser K B 1989 Design and preliminary tests of a beam intensity monitor for LEP *Proc. of Particle Accelerator Conf. 1989* (*Chicago, IL*) pp 71–73
[7] Nakamura K, Gonsalves A J, Lin C, Smith A, Rodgers D, Donahue R, Byrne W and Leemans W P 2011 Electron beam charge diagnostics for laser plasma accelerators *Phys. Rev. ST Acc. Beams* **14** 062801
[8] Spence D J and Hooker S M 2001 Investigation of a hydrogen plasma waveguide *Phys. Rev.* E **63** 015401
[9] Leemans W P, Nagler B, Gonsalves A J, Toth C, Nakamura K, Geddes C G R, Esarey E, Schroeder C B and Hooker S M 2006 GeV electron beams from a centimeter-scale accelerator *Nat. Phys.* **2** 696
[10] Gonsalves A J *et al* 2011 Tunable laser plasma accelerator based on longitudinal density tailoring *Nat. Phys.* **7** 862

[11] Leemans W P *et al* 2014 Multi-GeV electron beams from capillary-discharge-guided subpetawatt laser pulses in the self-trapping regime *Phys. Rev. Lett.* **113** 245002
[12] Choi H, Chae M S, Park S-J and Kang H-S 2014 Introduction to the test results of Turbo-ICT in PAL-ITF *Proc. Int. Beam Instrumentation Workshop 2014* (*Monterey, CA*) WEPF09 pp 553–7
[13] Gonsalves A J *et al* 2015 Generation and pointing stabilization of multi-GeV electron beams from a laser plasma accelerator driven in a pre-formed plasma waveguide *Phys. Plasmas* **22** 056703
[14] Stulle F and Bergoz J 2015 Turbo-ICT pico-coulomb calibration to percent-level accuracy *Proc. Free-Electron Lasers Conf. 2015* (*Daejeon*) MOP041
[15] Krishnan M, Elliott K W, Geddes C G R, van Mourik R A, Leemans W P, Murphy H and Clover M 2011 Electromagnetically driven, fast opening and closing gas jet valve *Phys. Rev. ST Acc. Beams* **14** 033502